doi:10.2533/chimia.2018.411 Chimia 72 (2018) 411–417

Spin-orbit Coupling Modulation in DNA by Mechanical Deformations

Solmar Varela Salazar[ab], Vladimiro Mujica*[c], and Ernesto Medina*[de]

Abstract: We consider molecular straining as a probe to understand the mobility and spin active features of complex molecules. The strength of the spin-orbit interaction relevant to transport in a low dimensional structure depends critically on the relative geometrical arrangement of current-carrying orbitals. Understanding the origin of the enhanced spin-orbit interaction in chiral systems is crucial to be able to control the spin selectivity observed in the experiments, which is a hallmark of the Chiral-Induced Selectivity Effect (CISS). Recent tight-binding orbital models for spin transport in DNA-like molecules, have surmised that the band spin-orbit (SO) coupling arises from the particular angular relations between orbitals of neighboring bases on the helical chain. Such arrangements could be probed by straining the molecule in a conductive probe AFM/Break junction type setup, as was recently reported by Kiran, Cohen and Naaman.[1] Here we report strain-dependent kinetic and SO coupling when a double-strand DNA model is compressed or stretched in two experimentally feasible setups with peculiar deformation properties. We find that the mobility and the SO coupling can be tuned appreciably by strain, and the analytical model bears out the qualitative trends of the experiments.

Keywords: Chiral-Induced Selectivity Effect (CISS) · DNA · Spin-orbit coupling

Solmar Varela Salazar obtained her Doctorate in Physics from the Central University of Venezuela in 2016. Her thesis was directed by Dr. Ernesto Medina and it was oriented to the study of electronic transport and spin transport in chiral organic molecules. Currently, she is a professor at the School of Chemical Sciences and Engineering of Yachay Tech, Ecuador, and she is a collaborator of the Mechanical Probe to Molecular Spintronics Project.

Vladimiro Mujica got his PhD at Uppsala University in 1985. He has been a Visiting Professor to the universities of Sao Paulo, Uppsala, Paris at Orsay, Tel-Aviv, Northwestern, Marseilles, KIAS, Fritz-Haber Institute, DIPC, NIST, and a Dresden Fellow In 2009 he joined the School of Molecular Sciences ASU. His areas of expertise include the theory of quantum relaxation and transport phenomena in mesoscopic system, molecular electronics, spintronics and nanophotonics. He has published over 150 peer-reviewed articles, with more than 5000 citations (h-index 32), and has been invited to more than 40 international conferences.

Ernesto Medina got his PhD at MIT in 1991. He has been a Visiting Professor to Rutgers University, Boston University, MIT, Lorraine University, Instituto de Materiales de Madrid among others. In 2016 he joined the School of Physical Sciences and Nanotechnology at Yachay Ecuador. His areas of recent interest include: molecular electronics and spintronics and proximity effects in low dimensional systems. He has published over 90 peer-reviewed articles, with more than 2000 citations, and has been invited to more than 20 international conferences.

*Correspondence: Prof. V. Mujica[c], Prof. E. Medina[de]
E-mail: vmujica@asu.edu; ernestomed@gmail.com
[a]Yachay Tech, School of Chemical Sciences & Engineering, 100119-Urcuquí, Ecuador
[b]Escuela de Física, Facultad de Ciencias, Universidad Central de Venezuela, Caracas, Venezuela
[c]School of Molecular Sciences, Arizona State University, Tempe, Arizona, 85287, USA
[d]Yachay Tech, School of Physical Sciences & Nanotechnology, 100119-Urcuquí, Ecuador
[e]Centro de Física, Instituto Venezolano de Investigaciones Cientí/ficas (IVIC), Apartado 21827, Caracas 1020 A, Venezuela

1. Introduction

Modifying local interactions in low dimensional systems by simple external means has been of continued interest in order to tailor material properties. Proximity effects, for example, are able to produce a variety of effects on graphene, from generating gaps,[2] to enhancing spin-orbit effects.[3,4] On the other hand, manipulating interactions in low dimensional systems, by mechanical deformations, has become known as stress engineering.[5,6] Here mechanical stretching results in effective $U(1)$ gauge fields or artificial 'magnetic fields' that act on conduction electrons. In the context of molecular electronics, a variety of experimental probes have been developed[7,8] that result in molecular deformations, for example in DNA and oligopeptides, whose effects have not been addressed in detail. In this paper, we address feasible stress manipulations on a simple model of DNA in order to vary the molecular couplings such as nearest neighbor hoppings and the spin-orbit (SO) interaction.

Chiral Induced Spin Selectivity (CISS) consists of the strong spin polarization of electrons when they are transmitted through a chiral structure. The CISS effect has been measured in a great variety of chiral molecular structures including single molecules of DNA,[8–10] Photosystem I,[11] self-assembled monolayers of DNA, chiral oligopeptides[12,13] and helicenes.[14] As these molecular systems lack strong exchange interactions and magnetic centers, it was first proposed that the spin-active ingredients to the photo-electron spin polarization setup[8] was the SO coupling[15] in addition to the chiral potential. Such couplings have been considered in recent theoretical models in order to describe transport of electrons through chiral molecules,[16–19] where the SO interaction has been introduced as resulting from some molecular electrostatic potential, without discussing the order of magnitude of the interaction required to account for the experimental results. Furthermore, some models[20,21] also include time reversal symmetry breaking features by either introducing coupling asymmetries between different conducting channels or adding dephasing by way of Buttiker voltage probe attachments[22] or otherwise introducing non-unitary effects.[23] These ingredients couple strongly to spin.[24]

Recently, in ref. [25], the SO coupling involved in transport is explicitly derived from a tight-binding model of DNA. The coupling is built from the overlap of *p* orbitals between vicinal bases and its magnitude depends on the DNA helix parameters (radius and pitch) and the relative positions of the orbitals. The magnitude of the SO interaction is derived ultimately from the atomic coupling from a perturbative treatment that connects nearest neighbor sites. Building on these results, we show here that it is possible to tune the magnitude of the SO interaction in a DNA helix model through changes in the radius and pitch due to the longitudinal deformations. Such deformations also modify the gap that protects spin polarized states during the transport process.[8,25] Recent experiments with oligopeptides[1] have shown that the capacity to filter spin, surmised to be associated to the SO coupling, is changed by compression in a conductive probe AFM set up (see also resistance studies of DNA with stretching[26]).

This work is organized as follows: In section 2 we derive the effective overlaps between nearest neighbor orbitals of a simple model of DNA. The effective overlaps are a result of the presence of the atomic spin-orbit coupling, using the Slater-Koster formulation[27,28] and a lowest-order matrix perturbation theory as proposed in ref. [29]. The effective SO coupling obtained recovers that of ref. [25] and depends explicitly on parameters that define the structural configuration of the DNA helix. The analysis of the behavior of the strength of the SO interaction under effects of longitudinal stretching and the experimentally reported Poisson ratio[30] are shown in section 3. The gap protecting spin transport reported in ref. [25] is also modulated by the structural parameters. It is shown that the SO strength is not optimal for the relaxed structure and can be enhanced by deformations. Furthermore, the detailed deformation dependence found can shed light on the orbitals involved in transport, making the CISS a spectral probe. We close with a summary and conclusions.

2. Analytical Slater-Koster Model for Double-stranded DNA

We model double-helix DNA as a helical sequence of steps (bases) whose plane is perpendicular to the molecular axis. The bases are planar ring-like structures with inplane sigma-bonding (sp^2) and out of plane orbitals (p_z-like) most likely to provide itinerant electrons.[31] Slater-Koster overlaps are considered between vicinal bases on each strand. The coupling between strands is considered very weak due to the relatively long distances implied by the hydrogen bonds. The direct overlap between neighboring p_z orbitals does not couple spin so additional couplings between the bare local orbitals must be considered. The atomic SO interaction couples the electron-bearing p_z orbitals to the sigma structure of the planar base, which in turn couples to the neighboring bases. In ref. [25] all lowest order couplings involving SO and external electric fields were considered as a function of the structural parameters of the double helix. The effective couplings were derived by solving the system of coupled equations for the elemental overlaps by a one-step decimation[32] procedure equivalent to the lowest-order perturbation.

Here we derive the effective Hamiltonian of the DNA incorporating spin coupling from the more compact approach of band folding.[29,33] We consider an intrinsic atomic SO coupling (associated to C or N for the DNA bases) given by

$$H_{\rm SO} = \frac{e\hbar}{4m_0^2c^2}\mathbf{s}\cdot(\mathbf{p}\times\nabla\mathbf{V}), \quad (1)$$

where m_0 is the effective electron mass, V is the atomic potential, $\mathbf{s}$ is the electron spin, $\hbar$ is Planck's constant, e the electron charge and c is the speed of light. Considering the bare p orbitals on the bases, the possible SO matrix elements between these orbitals are

	$\lvert p_x\rangle$	$\lvert p_y\rangle$	$\lvert p_z\rangle$
$\langle p_x\rvert$	0	$-i\boldsymbol{s}_z\xi_p$	$i\boldsymbol{s}_y\xi_p$
$\langle p_y\rvert$	$i\boldsymbol{s}_z\xi_p$	0	$-i\boldsymbol{s}_x\xi_p$
$\langle p_z\rvert$	$-i\boldsymbol{s}_y\xi_p$	$i\boldsymbol{s}_x\xi_p$	0

where $\xi_p = \lambda\hbar^2/2$. For carbon atoms $\xi_p \sim 6$ meV. $\mathbf{s}_i = \hbar/2\sigma_i$, with σ_i the Pauli matrices in the local orbital system. The eigenvalue equation for the coupled Hamiltonian is given by

$$\begin{pmatrix} H_\gamma & T \\ T^\dagger & H_\chi \end{pmatrix}\begin{pmatrix} \gamma \\ \chi \end{pmatrix} = E\begin{pmatrix} \gamma \\ \chi \end{pmatrix}. \quad (2)$$

Here H_γ is the sub-space that contains the p_z orbital site energies and the off-diagonal overlaps E_{zz} between the p_z orbitals on $\imath$ and j sites

$$H_\gamma = \begin{pmatrix} \epsilon_{2p}^\pi & E_{zz}^{\imath\jmath} \\ E_{zz}^{\jmath\imath} & \epsilon_{2p}^\pi \end{pmatrix}. \quad (3)$$

where ϵ_{2p}^π are the bare energies of $2p$ C levels. The T sub-space contains the intrinsic coupling between the p_z orbitals with orbitals p_x and p_y of the sigma-bonded carbon of the base and $E_{xz}^{\imath\jmath}$ and $E_{yz}^{\imath\jmath}$ overlaps between these orbitals on $\imath$ and j sites,

$$T = \begin{pmatrix} 0 & -i\boldsymbol{s}_y\xi_p & i\boldsymbol{s}_x\xi_p & 0 & E_{zx}^{\imath\jmath} & E_{zy}^{\imath\jmath} \\ 0 & E_{zx}^{\jmath\imath} & E_{zy}^{\jmath\imath} & 0 & -i\boldsymbol{s}_y\xi_p & i\boldsymbol{s}_x\xi_p \end{pmatrix}. \quad (4)$$

Finally, the H_χ sub-space contains the energies ϵ_s, ϵ_{2p}^σ and ϵ_{2p}^π of the s, $p_{x,y}$ and p_z orbitals of the nearest neighbor base.

$$H_\chi = \mathrm{diag}[\epsilon_s, \epsilon_{2p}^\sigma, \epsilon_{2p}^\sigma, \epsilon_s, \epsilon_{2p}^\sigma, \epsilon_{2p}^\sigma]. \quad (5)$$

The wave function subspaces $\Upsilon = (\psi_{\imath p_z}, \psi_{\jmath p_z})$ and $\chi = (\psi_s, \psi_{p_x}, \psi_{p_y})$ are coupled by T.

The matrix elements $E_{\mu\mu'}^{\sigma,\pi}$ that represent the overlaps of bare orbitals are expressed as a linear combination of Slater-Koster parameters $V_{\mu\mu'}^{\sigma,\pi}$ which are related to the different types of molecular bonding (σ, π) between the atomic wavefunctions of the μ and μ' orbitals.[29,34] These elements obey the commutation rule $V_{ll'} = (-1)^{l+l'}V_{l'l}$ where l is the orbital angular momentum quantum number ($l = 1$ for p orbitals). Harrison *et al.*[34] proposes an empirical expression for orbital overlaps as a function of the interatomic distance $\mathbf{R}_{\jmath\imath}$, given that

$$V_{\mu\mu'}^{\sigma,\pi} = \kappa_{\mu\mu'(\sigma,\pi)}\frac{\hbar^2}{m_e R_{\jmath\imath}^2}, \quad (6)$$

where $\kappa_{\mu\mu'}(\sigma,\pi)$ depends on the particular atom and

$$|\mathbf{R}_{j\imath}|^2 = \frac{16\pi^2 a^2 \sin^2(\Delta\phi/2) + (b\Delta\phi)^2}{4\pi^2}. \quad (7)$$

If separation of the atoms is large, the dependence on the distance is exponential.

As the bases rotate along the helix we must consider that the orbitals do not have the same absolute orientation at each site.[28] Using $\hat{\mathbf{X}}, \hat{\mathbf{Y}}, \hat{\mathbf{Z}}$ as the basis fixed in space, we define the unit vectors $\hat{\mathbf{n}}(\mu_j)$ in the direction the orbital μ_j living on the helix as

$$\hat{\mathbf{n}}(p_x, \imath) = \cos\phi_\imath \hat{\mathbf{X}} + \sin\phi_\imath \hat{\mathbf{Y}}, \quad (8)$$
$$\hat{\mathbf{n}}(p_y, \imath) = -\sin\phi_\imath \hat{\mathbf{X}} + \cos\phi_\imath \hat{\mathbf{Y}}, \quad (9)$$
$$\hat{\mathbf{n}}(p_z, \imath) = \hat{\mathbf{Z}}, \quad (10)$$

with $\phi_\imath = (\imath - 1)\Delta\phi$, where $\imath = 1...N$ and N is the total number of sites on helix. If the orbitals $\mu_\imath$ are located in $\mathbf{R}_\imath$ and the orbitals μ' are in $\mathbf{R}_j$, overlap between the orbitals at $\imath$ and j sites are given by

$$E^{\imath,\jmath}_{\mu\mu'} = (\hat{\mathbf{n}}(\mu_\imath), \hat{\mathbf{n}}(\mu'_\jmath))V_{\mu\mu'} \quad (11)$$
$$+\frac{(\mathbf{R}_{j\imath}, \hat{\mathbf{n}}(\mu_\imath))(\mathbf{R}_{j\imath}, \hat{\mathbf{n}}(\mu'_\jmath))}{(\mathbf{R}_{j\imath}, \mathbf{R}_{j\imath})}\left(V^\sigma_{\mu\mu'} - V^\pi_{\mu\mu'}\right), \quad (12)$$

where $\mathbf{R}_{j\imath} = \mathbf{R}_j - \mathbf{R}_\imath$ the vector connecting the $\imath$ and j sites. By Eqn. (12) we obtain that matrix elements are

$$E^{\imath\jmath}_{zz} = V^\pi_{pp} + \frac{b^2(\Delta\phi)^2(V^\sigma_{pp} - V^\pi_{pp})}{4\pi^2|\mathbf{R}_{j\imath}|^2} = E^{\imath\jmath}_{zz}, \quad (13)$$

$$E^{\imath\jmath}_{xz} = \frac{2ab\nu_{\imath\jmath}\sin^2\left(\frac{\Delta\phi}{2}\right)\Delta\phi(V^\sigma_{pp} - V^\pi_{pp})}{2\pi|R_{j\imath}|^2} = -E^{\jmath\imath}_{zx} \quad (14)$$

where $\nu_{ij} = sgn(j - \imath)$ and

$$E^{\imath\jmath}_{yz} = \frac{ab\Delta\phi\sin\Delta\phi\left(V^\sigma_{pp} - V^\pi_{pp}\right)}{2\pi|\mathbf{R}_{j\imath}|^2} = E^{\jmath\imath}_{zy}. \quad (15)$$

The dependence of the overlaps on the geometric properties of the helix, *i.e.* pitch b, rotation angle between bases $\Delta\phi$, and helix radius a will parameterize the molecular deformations and determine the coupling strengths.

Decimating the subspace χ and retaining up to linear terms in E and lowest order in the coupling T (Eqn. 2), we obtain that effective Hamiltonian by the relation[29,33]

$$H = S^{-1/2}\left[H_\gamma - TH_\chi^{-1}T^\dagger\right]S^{-1/2}, \quad (16)$$

where $S = 1 + TH_\chi^{-1}T^\dagger$.

The product $TH_\chi^{-1}T^\dagger$ is expanded as

$$TH_\chi^{-1}T^\dagger = \begin{pmatrix} 0 & -is_y\xi_p & is_x\xi_p & 0 & E^{\imath\jmath}_{zx} & E^{\imath\jmath}_{zy} \\ 0 & E^{j\imath}_{zx} & E^{j\imath}_{zy} & 0 & -is_y\xi_p & is_x\xi_p \end{pmatrix} \begin{pmatrix} \frac{1}{(\epsilon^\pi_{2p}-\epsilon_s)} & 0 & 0 & 0 & 0 & 0 \\ 0 & \frac{1}{(\epsilon^\pi_{2p}-\epsilon^\sigma_{2p})} & 0 & 0 & 0 & 0 \\ 0 & 0 & \frac{1}{(\epsilon^\pi_{2p}-\epsilon^\sigma_{2p})} & 0 & 0 & 0 \\ 0 & 0 & 0 & \frac{1}{(\epsilon^\pi_{2p}-\epsilon_s)} & 0 & 0 \\ 0 & 0 & 0 & 0 & \frac{1}{(\epsilon^\pi_{2p}-\epsilon^\sigma_{2p})} & 0 \\ 0 & 0 & 0 & 0 & 0 & \frac{1}{(\epsilon^\pi_{2p}-\epsilon^\sigma_{2p})} \end{pmatrix} \begin{pmatrix} 0 & 0 \\ is_y\xi_p & E^{\imath\jmath}_{xz} \\ -is_x\xi_p & E^{\imath\jmath}_{yz} \\ 0 & 0 \\ E^{j\imath}_{xz} & is_y\xi_p \\ E^{j\imath}_{yz} & -is_x\xi_p \end{pmatrix}. \quad (17)$$

Replacing Eqn. (17) into Eqn (16) and approximating $S \sim 1$, the effective Hamiltonian is

$$H \approx H'_\gamma - \begin{pmatrix} \frac{2\xi_p^2 + (E^{\imath\jmath}_{zx})^2 + (E^{\imath\jmath}_{zy})^2}{(\epsilon^\pi_{2p} - \epsilon^\sigma_{2p})} & \frac{2i\xi_p s_y E^{\imath\jmath}_{zx}}{(\epsilon^\pi_{2p} - \epsilon^\sigma_{2p})} \\ -\frac{2i\xi_p s_y E^{\imath\jmath}_{zx}}{(\epsilon^\pi_{2p} - \epsilon^\sigma_{2p})} & \frac{2\xi_p^2 + (E^{\imath\jmath}_{zx})^2 + (E^{\imath\jmath}_{zy})^2}{(\epsilon^\pi_{2p} - \epsilon^\sigma_{2p})} \end{pmatrix}, \quad (18)$$

where H'_γ is the subspace with $\epsilon^\pi_{2p} = 0$, where we have used the symmetry relations

$$E^{\imath\jmath}_{xz} = -E^{\imath\jmath}_{zx} = -E^{j\imath}_{xz}, \quad E^{\imath\jmath}_{yz} = E^{\imath\jmath}_{zy} = E^{j\imath}_{yz}. \quad (19)$$

Terms on the diagonal of Eqn. (18) give both corrections to the p_z orbital energy and the effective coupling between p_z orbitals. Using expressions (7)–(13), the Hamiltonian for the full Brillouin zone can be written as

$$H = t\sum_{\langle\imath\jmath\rangle} c_\imath^\dagger c_\jmath + i\lambda_{\rm SO}\sum_{\langle\imath\jmath\rangle} c_\imath^\dagger \nu_{\imath\jmath}\mathbf{s}_y c_\jmath, \quad (20)$$

where

$$t = E_{zz} = V^\pi_{pp} + \frac{b^2\Delta\phi^2\left(V^\sigma_{pp} - V^\pi_{pp}\right)}{8\pi^2a^2(1-\cos\Delta\phi) + b^2\Delta\phi^2} \quad (21)$$

is the kinetic term, and

$$\lambda_{\rm SO} = \frac{8\pi\xi_p ab\Delta\phi\sin^2\left(\frac{\Delta\phi}{2}\right)\left(V^\sigma_{pp} - V^\pi_{pp}\right)}{\left(\epsilon^\pi_{2p} - \epsilon^\sigma_{2p}\right)\left(16\pi^2a^2\sin^2\left(\frac{\Delta\phi}{2}\right) + b^2\Delta\phi^2\right)}, \quad (22)$$

is the effective intrinsic SO coupling, recovering the expressions derived in ref. [25]. Here the two helices are uncoupled so we will have two identical copies of the same Hamiltonian translating into two channels for transport. In order to estimate the contribution of $V^\sigma_{pp} - V^\pi_{pp}$ we will use Eqns. (6) and (7).

One salient feature of the $\lambda_{\rm SO}$ is how the atomic SO is translated to transport. The strength of the interaction, as in graphene, depends critically on the relative positions of the orbitals involved: when the pitch of the molecule is reduced, the SO coupling is linearly reduced, and disappears for zero pitch b, where the bases would be on the same plane. The sensitive role of the geometry can power up the interaction a few orders of magnitude, as happens in graphene, where the flat sheet has a SO coupling of μeV (where both geometry and interference are involved), while nanotubes, as rolled sheets of graphene, have a coupling of *me*V.[35] A similar effect would be seen if we slightly unwind the helix reducing the rotation angle $\Delta\phi$, as can be seen from Eqn. (22) for $\lambda_{\rm SO}$.

3. Stretching Effects on SO Coupling

In this section we will derive the effects on the SO strength, of feasible experimental deformations. As shown in ref. [1], *conductive probe AFM* can be used to tip-load an oligopeptide and modulate its spin filtering capacity. Different types of loadings could reveal further interesting features for the orbital overlaps involved in spin-filtering and, most interestingly, the source of transport SO coupling. Deformation response could also yield some clarifications regarding the interpretations of conductance histograms/I-V curve statistics when a molecule is placed in a conductive probe setup.

For the first type of loading (see refs [8, 36] and references therein) we fix both strands on one end of the DNA while the other end is free to rotate, being attached, for example, to a bead in an optical trap. This way the rotation angle $\Delta\phi$ changes, keeping the radius constant. The second loading setup constrains both ends, leaving no rotational freedom and assumes the effective elastic behavior is like a body with a Poisson ratio with a fixed rotational angle per base.

3.1 *Stretching with a Free Rotating End*

A simple model for twisted DNA is to consider that the distance along the sugar backbone, between bases R_{ij} with i and j nearest neighbors, is kept constant (by the rigidity of the DNA backbone). The twisting of the structure is then mediated by the repulsion of the π clouds projected from the bases themselves. Any untwisting by pulling, here at fixed radius a_0 (see Fig.1) then costs energy because the p_z electron clouds change their overlap. This model implies a particular relation between pitch and rotation per base of the form (see Eqn. (7))

$$b = \frac{2\pi}{\Delta\phi} R_{ij} \sqrt{1 - 4\left(\frac{a_0}{R_{ij}}\right)^2 \sin^2(\Delta\phi/2)} \quad (23)$$

where we recall that a is the radius of the helix that is kept constant for any twisting angle. The length of the chain is related to the pitch b of the helix by $L = (N-1)\, b\Delta\phi/2\pi$ where N is the number of base pairs in the chain. The strain on the molecule is defined as $\varepsilon = (L - L_0)/L_0 = \Delta L/L_0$, where L_0 and L are the initial and final length of the double helix, respectively. The pitch, after a strain ε, will be $b(\varepsilon) = 2\pi L_0(1+\varepsilon)/\Delta\phi(N-1)$. The strain changes the angle $\Delta\phi$ that separates two consecutive bases in the double helix. Using the previous relations we can solve for $\Delta\phi$ as

$$\Delta\phi(\varepsilon) = 2\arcsin\left(\frac{\sqrt{[R_{pi}(N-1)]^2 - L_o^2(1+\varepsilon)^2}}{2a_o(N-1)}\right). \quad (24)$$

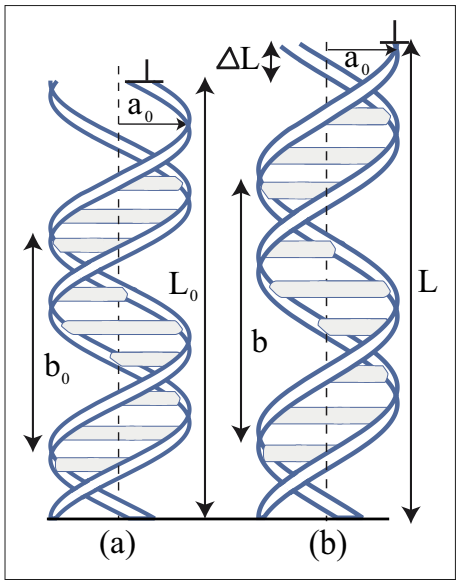

Fig. 1. (a) Schematic illustration of the deformation of the DNA helix at fixed radius a_0 and variable pitch b. (b) After ΔL deformation, with one free end, the helix elongate by twisting at constant radius, as described in the text.

The magnitude of the SO interaction is then

$$\lambda_{SO}(\varepsilon) = \frac{32\pi\hbar^2\xi_p(\kappa^{\sigma}_{pp} - \kappa^{\pi}_{pp})a_0 L_0(1+\varepsilon)\Delta\phi(\varepsilon)\sin^2\left(\frac{\Delta\phi(\varepsilon)}{2}\right)}{m(\epsilon^{\pi}_{2p} - \epsilon^{\sigma}_{2p})\left(16\pi^2 a_0^2 \sin^2\left(\frac{\Delta\phi(\varepsilon)}{2}\right) + b_0^2(1+\varepsilon)^2\Delta\phi(\varepsilon)^2\right)}. \quad (25)$$

Let us consider a double helix with N = 11 base pairs with undeformed $\Delta\phi = \pi/5$, and $L_0 = b_0$. The value of L_0 is obtained using the values $a = a_0 = 11.85 \times 10^{-10}$ m = 22.39 au (atomic units)).

Fig. 2 depicts the behavior of the SO coupling as a function of the deformation with twisting for a large range of strains. The inset depicts a physical range of possible ε values and shows that pulling ($\varepsilon > 0$) on the molecule slightly enhances the SO coupling while compressing it, without accounting for possible sideways bending, slightly reduces the SO coupling (10% change either way). On the other hand, Fig. 3 shows that the kinetic term, in the physical range, is reduced in magnitude on stretching while it is enhanced on compression. Mobility and SO strength are then at odds when deformations are considered in this configuration.

3.2 *Stretching with both Ends fixed*

For our second straining setup, we consider stretching or compression of DNA assuming that the orbitals on the bases do not change their orientation and $\Delta\phi$ remains invariant during the deformation process. This is achieved when both the ends of the molecule are fixed with no rotational freedom. We then considered DNA as an elastic body with a Poisson ratio as has been reported in experiments.[30]

For a helix DNA with $\mathcal{N}$ turns and N bases in total, the length of the chain can be written as

$$L = \frac{(N-1)\Delta\phi}{2\pi} b = \mathcal{N} b. \quad (26)$$

Using Poisson's ratio for DNA equal to ν and considering a longitudinal deformation $\varepsilon = \Delta L/L_0$, SO interaction changes as

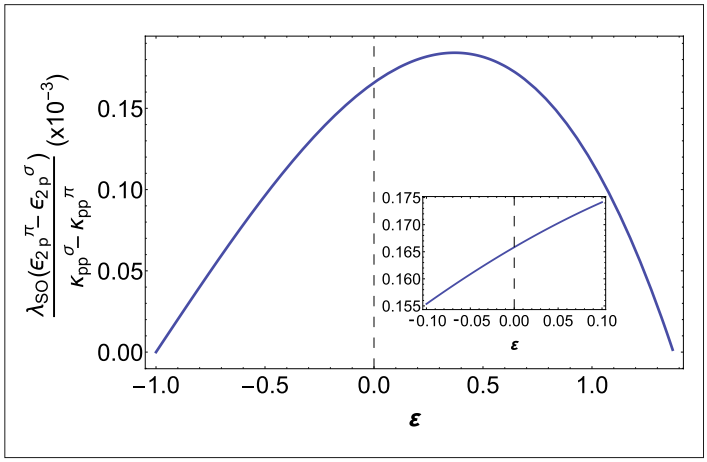

Fig. 2. λ_{so} versus the strain ε for the one free end configuration. Stretching enhances while compressing degrades the SO coupling. The inset shows the change in the SO coupling in a physical range of deformations for the DNA of 11 base pairs. The ratio $(\kappa^{\sigma}_{pp} - \kappa^{\pi}_{pp})/(\epsilon^{\pi}_{2p} - \epsilon^{\sigma}_{p})$ is a constant only relating to the nature of the bonded orbitals.

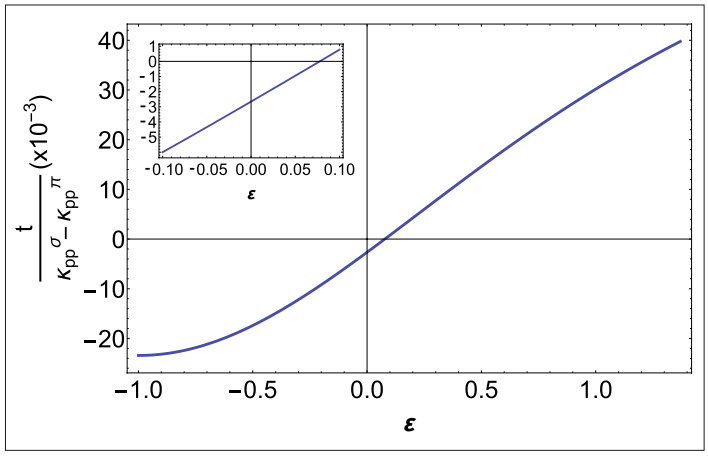

Fig. 3. The kinetic energy parameter t versus the strain ε. Note that the absolute value of the nearest neighbor coupling is reduced on stretching while it is enhanced on compression.

$$\lambda_{\rm SO}(\Delta L) = \frac{32\pi\frac{\hbar^2}{m}\xi_p(\kappa^{\sigma}_{pp}-\kappa^{\pi}_{pp})a_0\,(1-\nu\varepsilon)\left(b_0+\frac{\varepsilon L_0}{\mathcal{N}}\right)\Delta\phi\sin^2\left(\frac{\Delta\phi}{2}\right)}{\left(\epsilon^{\pi}_{2p}-\epsilon^{\sigma}_{2p}\right)\left(16\pi^2a_0(1-\nu\varepsilon)^2\sin^2\left(\frac{\Delta\phi}{2}\right)+(b_0+\frac{\varepsilon L_0}{\mathcal{N}})^2\Delta\phi^2\right)^2}, \quad (27)$$

where a_0 is the radius and L_0 is the length of the DNA molecule without stretching and ΔL is the change of length during deformation. If $\Delta L < 0$ ($\Delta L > 0$) the molecule is compressed (stretched) in the longitudinal direction and radius increases (decreases) (Fig. 4). The ratio $(\kappa^{\sigma}_{pp}-\kappa^{\pi}_{pp})/(\epsilon^{\pi}_{2p}-\epsilon^{\sigma}{}_{p})$ is a constant only relating to the nature of the bonded orbitals.

Fig. 5 displays the SO magnitude versus the longitudinal deformation ε. ε varies in interval –1 to $1/\nu$. We emphasize some particular features of the overlaps: When ε = –1, the helix is completely compressed, the pitch b being zero and the resulting structure is a ring with $a = a_0(1+\nu)$. In this case, the SO magnitude is zero because the E^{vj}_{xz} overlaps disappear killing the SO interaction. On the other hand, when ε approaches $1/\nu$, the pitch b is large compared to the helix radius a, the SO interaction weakens because overlaps depend on the inverse of the separation between the bases. At a particular value for ε the SO coupling is a maximum as a function of ε where b and a are coupled by the Poisson ratio.

The Poisson ratio for dsDNA is reported to be $\nu = 0.5$ in experiments.[30] For this value $\varepsilon = 0.57$ yields and maximum for the SO magnitude and its value is approximately 52% greater than the value without deformation. Note that compressing the double helix would yield a decrease of the SO coupling. These behaviors could be tested in detailed experiments, to verify the origin of the SO coupling and the orbital overlaps involved in transport. Nevertheless, Fig. 5 shows a broader range of stretching than can actually be achieved without breaking the molecule. According to measurements performed on DNA, molecules between 5 and 25 base pairs can only be stretched 1.4 to 1.6 Å. To show a more realistic range for stretching, we depict the SO coupling changes in the inset of Fig. 5.

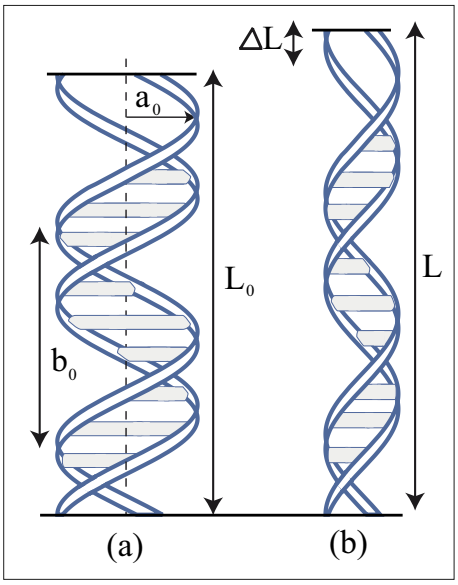

Fig. 4. (a) Schematic illustration of the deformation of the DNA helix of radius a_0 and pitch b_0. (b) After ΔL deformation, the radius and pitch change as $a = a_o - \nu a_o \Delta L/L_o$ and $b = b_o + \Delta L/\mathcal{N}$, respectively.

4. Effects of DNA Deformation on the SO Gap

From the Hamiltonian described in Eqn. (20) one can derive the corresponding Bloch Hamiltonian. Our model of DNA assumes that transport electrons are available on the $2p - \pi$ orbitals of the bases. These orbitals have one unpaired electron, so we choose to describe the Bloch physics of the half-filled model. The corresponding Hamiltonian in the vicinity of this point is

$$H = -2\nu q_y R t - 2\nu\lambda_{\rm SO}\boldsymbol{s}_y, \quad (28)$$

where q_y is the wave-vector measuring the separation from half filling in reciprocal space in the rotating frame with respect to the fixed $\hat{\mathbf{X}}, \hat{\mathbf{Y}}, \hat{\mathbf{Z}}$ reference frame (see Eqn. (10)), R is given by Eqn. (7) and ν is a quantum number denoting the sense of rotation of electrons on the helix. Writing the operator $\boldsymbol{s}_y$ in the rotating frame one arrives at the Hamiltonian[25]

$$H_{helix} = \nu\begin{pmatrix} iT\partial_\varphi & 2i\lambda_{\rm SO}e^{-i\varphi} \\ -2i\lambda_{\rm SO}e^{i\varphi} & iT\partial_\varphi \end{pmatrix}, \quad (29)$$

written in spin space in the rotating frame, where $T = 2Rt$. The eigenvalues associated with the energy are given by

$$E^{\nu,\zeta}_{n,s} = \begin{cases} \frac{|T|n}{2M\mathcal{N}}, & \lambda_{\rm SO}=0 \\ \frac{|T|n}{2M\mathcal{N}} - s\nu\frac{\sqrt{T^2+(4\lambda_{\rm SO})^2}}{2}, & \lambda_{\rm SO}\neq 0 \end{cases}, \quad (30)$$

with $\mathcal{N}$ the number of turns in the helix, M the number of bases per turn, n that gives the subbands corresponding to the discrete modes due to longitudinal confinement within a helix[37] and $s\nu$ is the helicity of the electron associate to the spin component s. Note the singular behavior due to different symmetries of models with and without the SO coupling in the limit $\lambda_{\rm SO} \to 0$. The two cases have to be derived separately. This model predicts a gap Δ that separates the different helicities for the same direction of transport given by

$$\Delta = |T|\left(\sqrt{1+\left(\frac{4\lambda_{\rm SO}}{T}\right)^2} - \frac{1}{2\mathcal{N}}\right), \quad (31)$$

for $\lambda_{\rm SO} \neq 0$. If $\lambda_{\rm SO} = 0$ then $\Delta = 0$ and the states of different helicity are degenerate as expected. As shown in ref. [25] this gap protects spin states as in topological insulators and is a critical ingredient for spin filtering once time-reversal is broken by *e.g.* an external bias. In Fig. 6 we show the gap Δ given by Eqn. (31) as a function of molecular stretching. We note that the dependencies reflected in Fig. 6 result from both changes in T (through t in Eqn. (21)), the kinetic term, and the SO coupling. The gap gets a much more pronounced increase when stretching as opposed to compressing (with a slight offset). The latter offset becomes important when looking at physical range parameters according to ref. [26], as shown in the inset of Fig. 6. The gap has a non-monotone dependence on stretching while it can be enhanced by compressing the molecule.

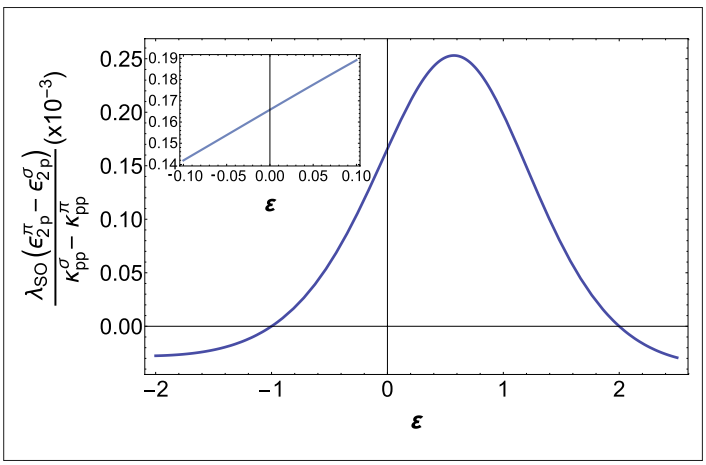

Fig. 5. $\lambda_{\rm SO}$ normalized by $(\kappa^{\sigma}_{pp}-\kappa^{\pi}_{pp})/(\epsilon^{\pi}_{2p}-\epsilon^{\sigma}{}_{p})$ versus the deformation ε of a DNA helix. The plot shows that stretching can enhance the SO coupling, while compressing weakens the coupling. The inset shows a more realistic range for ε according to ref. [26].

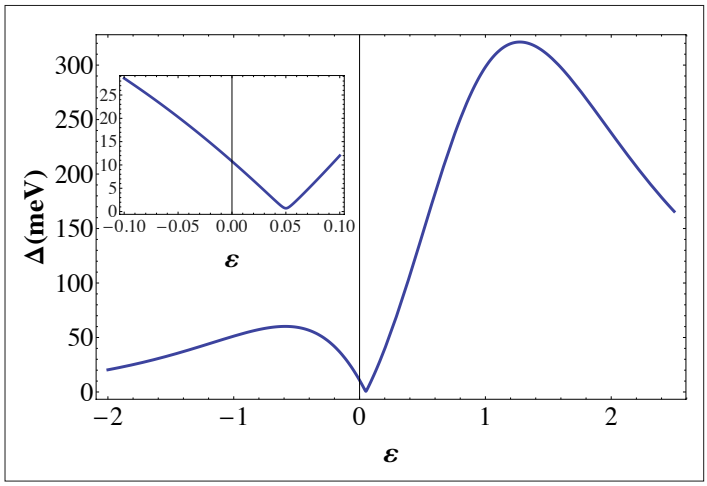

Fig. 6. SO gap versus deformation of a helix of dsDNA. The figure shows the general trend for a wide range of values of ε while the inset emphasizes the physical range of deformations according to ref. [26]. We have taken the values of $\kappa_{pp\sigma}$ =3.24, $\kappa_{pp\pi}$ =-0.81 from ref. [34].

This gap is also sensitive to the number of turns in the molecule, as shown in Fig. 7.

5. Summary and Conclusions

We have developed a model for the strain dependence of the spin orbit coupling in double-stranded DNA. In the model we assumed that transport electrons are provided by p_z orbitals from 2*p* levels that are projected perpendicular to the base molecules. The source of the SO coupling is atomic, associated to carbon and nitrogen atoms in the base pairs of the double helix. We derived the molecular Hamiltonian by using the Slater-Koster tight-binding approach in the rotating frame. The spin-orbit coupling is derived explicitly in terms of the atomic SO interaction (one orbital per base) and the orbital overlaps between nearest neighbor bases along each helix of double-stranded DNA. Coupling between strands is only mechanical and no transport between strands is considered.

Having the SO coupling as a function of the geometrical parameters of the DNA we are able to compute the changes in both the kinetic energy and the SO coupling by longitudinal deformations of the molecule. Two strain scenarios are considered i) strain with one end free to rotate at fixed double helix radius, and ii) straining with fixed ends, considering the molecule as an elastic body. The relation between pitch and radius as strain occurs is controlled by the experimentally reported Poisson ratio for DNA.

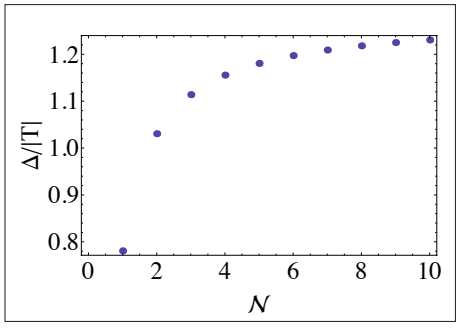

Fig. 7. SO gap in units of the kinetic energy |T| versus the length of the helix. The energy gap separating the spin up states from spin down states, for a given helicity, increases with the length of the helix for fixed a and b.

We find that stretching DNA increases the SO coupling by at least 10% in both straining configurations considered while the kinetic energy terms in the molecular Hamiltonian are reduced in the same range of parameters. On the other hand compressing uniaxially (no bending effects) reduces the SO coupling. One is then able to significantly manipulate spin active interaction by straining and we report the same trends as in experiments,[1] qualitatively validating the proposed tight binding model. We clarify that the helicoidal arrangement of the π orbitals on the bases itself, is an activating geometry for the SO coupling.[25] A planar ring arrangement would not be SO active according to our model. This fact is also familiar in flat graphene where the SO is a second neighbors coupling turning it into a μeV size effect.

We also derive the dependence of the SO gap discussed in ref. [25] and its dependence on straining. The SO gap is affected both by changes in the kinetic term and the SO coupling. We find that while stretching reduces the gap, compressing can increase its value by a factor of two in the physical strain range. Changes in the gap are more revealing of the filtering capacity of the molecule than the values of the SO coupling alone. Experiments using conductive probe AFM[1,26] could directly verify our results and help settle the question of the source of the SO coupling and the conduction electrons in dsDNA. It is important to note an observation of Bruot *et al.*[26] on the distribution of deformation of a helical molecule based on the De Gennes elastic model:[38] induced deformations will be non-uniform and concentrated at the ends of the molecule. A feature to contemplate in future detailed modelling of stretching effects on spin transport.

As a final remark, we note that the considerations in this work broaden our understanding of conductive probe measurements using both AFM and break junction setups that can involve molecular straining during transport measurements. As an example, conductance histogram interpretation could go beyond identifying the peak values.

Acknowledgements

We thank Henry Pinto and Duncan Mowbray for illuminating discussions. This work was supported by internal grant 30-2017 'Mechanical Spectroscopy' of Yachay Tech University.

Received: April 23, 2018

[1] V. Kiran, S. R. Coleman, R. Naaman, *J. Chem. Phys.* **2017**, *146*, 092302.
[2] A. Hallal, F. Ibrahim, H. Yang, S. Roche, M. Chshiev, *2D Materials* **2017**, *4*, 025074.
[3] A. Varykhalov, J. Sanchez-Barriga, A. M. Shikin, C. Biswas, E. Vescovo, A. Rybkin, D. Marchenko, O. Rader, *Phys. Rev. Lett.* **2008**, *101*, 157601.
[4] D. Marchenko, A. Varykhalov, M. R. Scholz, G. Bihlmayer, E. I. Rashba, A. Rybkin, A. M. Shikin, O. Rader, *Nat. Comm.* **2012**, *3*, 1232.
[5] F. Guinea, B. Horovitz, P. Le Doussal, *Phys. Rev. B* **2008**, *77*, 205421.
[6] M. A. H. Vozmediano, M. I. Katsnelson, F. Guinea, *Phys. Rep.* **2010**, *496*, 109.
[7] a) M. Loiacono, E. Granstrom, C. Frisbie, *J. Phys. Chem B* **1998**, *102*, 1679; b) B. Xu, N. J. Tao, *Science* **2003**, *301*, 1221; c) N. J. Tao, *Nat. Nanotech.* **2006**, *1*, 173.
[8] Z. Xie. T. Z. Markus, S. R. Cohen, Z. Vager, R. Gutierrez, R. Naaman, *Nano Lett.* **2011**, *11*, 4652.
[9] B. Göhler, V. Hamelbeck, T. Z. Markus, M. Kettner, G. F. Hanne, Z. Vager, R. Naaman, H. Zacharias, *Science* **2011**, *331*, 894.
[10] S. Ravi, P. Sowmiya, A. Karthikeyan, *Spin* **2013**, *3*, 13500031.
[11] I. Carmeli, K. S. Kumar, O. Hieflero, C. Carmeli, R. Naaman, *Angew. Chem. Int. Ed.* **2014**, *126*, 9099.
[12] M. Kettner, B. Göhler, H. Zacharias, D. Mishra, V. Kiran, R. Naaman, C. Fontanesi, D. H. Waldeck, S. Sek, J. Pawlowski, J. Juhaniewicz, *J. Phys. Chem. C* **2015**, *119*, 14542.
[13] A. C. Aragones, E. Medina, M. Ferrer-Huerta, N. Gimeno, M. Teixidó, J. L. Palma, N. Tao, J. M. Ugalde, E. Giralt, I. Díez-Pérez, V. Mujica, *Small* **2017**, *13*, 1602519.
[14] V. Kiran, S. P. Mathew, S. R. Cohen, I. H. Delgado, J. Lacour, R. Naaman, *Adv. Mater.* **2016**, *28*, 1957.
[15] S. Yeganeh, M. A. Ratner, E. Medina, V. Mujica, *J. Chem. Phys.* **2009**, *131*, 014707.
[16] S. Varela, E. Medina, F. Lopez, V. Mujica, *J. Phys. Cond. Mat.* **2014**, *26*, 015008.
[17] E. Medina, F. Lopez, M. Ratner, V. Mujica, *Europhys. Lett.* **2012**, *99*, 17006.
[18] R. Gutierrez, E. Díaz, C. Daul, T. Brumme, F. Domínguez-Adame, G. Cuniberti, *J. Phys. Chem. C* **2013**, *117*, 22276.
[19] K. Michaeli, R. Naaman, e-print arXiv:1512.03435v2 [cond-mat.mes-hall], **2016**.

[20] R. Gutierrez, E. Díaz, R. Naaman, G. Cuniberti, *Phys. Rev. B* **2012**, *85*, 081404(R).
[21] A.-Min Guo, Q.-F Sun, *Phys. Rev. Lett.* **2012**, *108*, 218102.
[22] A.-Min Guo, Q.-F Sun, *PNAS* **2014**, *111*, 11658.
[23] S. Matityahu, Y. Utsumi, A. Aharony, O. Entin-Wohlman, C. A. Balseiro, *Phys. Rev. B* **2016**, *93*, 075407.
[24] R. A. Caetano, *Sci. Rep.* **2016**, *6*, 23452.
[25] S. Varela, V. Mujica, E. Medina, *Phys. Rev. B* **2016**, *93*, 155436.
[26] C. Bruot, L. Xiang, J. L. Palma, N. Tao, *ACS Nano* **2014**, *9*, 88.
[27] J. C. Slater, G. F. Koster, *Phys. Rev.* **1954**, *94*, 1498.
[28] T. Ando, *J. Phys. Soc. Jpn.* **2000**, *69*, 1757.
[29] M. Peralta, L. Colmenarez, A. López, B. Berche, E. Medina, *Phys. Rev. B* **2016**, *94*, 235407.
[30] S. K. Gupta, A. McEwan, I. Lukacevic, *Phys. Lett. A* **2016**, *380*, 207.
[31] L. G. D. Hawke, G. Kalosakas, C. Simserides, *Mol. Phys*. **2009**, *107*, 1755.
[32] H. M. Pastawski, E. Medina, *Rev. Mex. Fís.* **2001**, *47*, S1.
[33] E. McCann, M. Koshino, *Rep. Prog. Phys*. **2013**, *76*, 056503.
[34] W. A. Harrison, 'Electronic Structure and the Properties of Solids', 2nd edition, Dover, New York, **1989**.
[35] T. Ando, *J. Phys. Soc. Jpn.* **2000**, *69*, 1757.
[36] D. Hern Paik, T. T. Perkins, *J. Am. Chem. Soc.* **2011**, *133*, 3219.
[37] I. Tinoco, R. W. Woody, *J. Chem. Phys.* **1964**, *40*, 160.
[38] P.-G. de Gennes, *C. R. Acad. Sci., Ser. IV: Phys., Astrophys.* **2001**, *2*, 1505.